Unusual, pH-Induced, Self-Assembly Of Sophorolipid Biosurfactants

Niki Baccile,[†,‡,§,*] Florence Babonneau,[†,‡,§] Jacques Jestin,[⊥] Gerard Pehau-Arnaudet,[∥] and Inge Van Bogaert[#]

[†]UPMC Université Paris 06, UMR 7574, Chimie de la Matière Condensée de Paris, F-75005, Paris, France, [‡]CNRS and [§]Collège de France, UMR 7574, Chimie de la Matière Condensée de Paris, F-75005, Paris, France, [⊥]Laboratoire Léon Brillouin, LLB, CEA Saclay, F-91191 Gif-sur-Yvette Cedex, France, [∥]Plate-Forme de Cryomicroscopie Moléculaire, URA 2185, Institut Pasteur, F-75015, Paris, France, and [#]InBio, Department of Biochemical and Microbial Technology, Faculty of Bioscience Engineering, Ghent University, 9000, Ghent, Belgium

ABSTRACT An increasing need exists for simple, bioderived, nontoxic, and up-scalable compounds with stimuli-responsive properties. Acidic sophorolipids (SL) are glucose-based biosurfactants derived from the yeast broth of *Candida bombicola* (teleomorph: *Starmerella bombicola*). The specific design of this molecule, a sophorose head with a free end-COOH group at the end of the alkyl chain, makes it a potentially interesting pH-responsive compound. We have specifically investigated this assumption using a combination of small angle neutron scattering (SANS), transmission electron microscopy under cryogenic conditions (Cryo-TEM), and nuclear magnetic resonance (NMR) techniques and found a strong dependence of SL self-assembly on the degree of ionization, α, of the COOH group at concentration values as low as 5 and 0.5 wt %. At least three regimes can be identified where the supramolecular behavior of SL is unexpectedly different: (1) at low α values, self-assembly is driven by concentration, *C*, and micelles are mainly identified as nonionic objects whose curvature decreases (sphere-to-rod) with *C*; (2) at mid α values, the formation of COO^- groups introduces negative charges at the micellar surface inducing an increase in curvature (rod-to-sphere transition). Repulsive electrostatic long-range interactions appear at this stage. In both regimes 1 and 2, the cross-section radius of the micelles is below 25 Å. This behavior is concentration independent. (3) At $\alpha = 1$, individual micelles seem to favor the formation of large netlike tubular aggregates whose size is above 100 nm. Such a complex behavior is very unique as it is generally not observed for common alkyl-based surfactants in concentration ranges below 5−10 wt %.

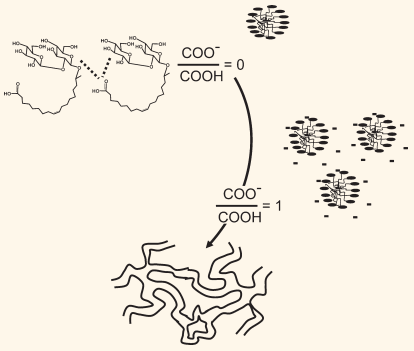

KEYWORDS: self-assembly · biosurfactants · ionization degree · pH-responsive · microbial-derived surfactants · sophorolipids · small angle neutron scattering · cryo-TEM

Stimuli-responsive surfactants are a class of compounds which have recently attracted major interest in polymer chemistry and material science. The control of the aggregation state, phase behavior, and surface tension at will has stimulated much effort both in fundamental and applied science. Stabilization of emulsions, suspensions or foams, drug encapsulation and delivery, hard-surface cleaning, personal care applications, surface charge variations, wettability control, enhancement of viscoelastic properties, recyclability, heat-transfer fluids, drag-reduction agents, and dynamic templates for nanomaterial synthesis are just some of the possible applications, while temperature, electric field, ionic strength, and pH are commonly studied "switches". pH, in particular, is a simple tool that induces different aggregation states of a given molecule. Classical commercial surfactants are either ionic (cationic, anionic, zwitterionic) or nonionic and do not show a strong pH-sensitive behavior. Actually, for some ester and amide-based compounds, pH represents a source of molecular disruptor. Block copolymers have larger sizes and good thermal stability and are promising tools in drug delivery applications because of their high loading capacity of active compounds; additionally, some of them have very interesting pH-responsive properties. In particular, poly(acrylic acid) (PAA)-based block copolymers are known to form pH-sensitive nanostuctures.[1,2] Nevertheless, their physicochemical behavior is strongly dependent on the chemical nature and size of the hydrophobic block; for example, adsorption and assembly kinetics are quite slow for poly(styrene), PS, or poly(*n*-butyl acrylate), PBA, based blocks,[2] and that is the case for many block copolymer-based systems; for this reason, interest in finding pH-responsive systems based on small amphiphiles is still high. Common surfactants made of an aliphatic chain (e.g., CTAB, SDS, Brij, *etc.*) show typical lyotropic properties but no specific pH-driven assembly effects, except for a few compounds, like oleyldimethyamine oxide[3] and some interesting cases of binary systems. In two recent examples, cetyltrimethylammonium bromide, CTAB, used in the presence of

* Address correspondence to niki.baccile@upmc.fr.

Received for review December 15, 2011 and accepted May 10, 2012.

Published online May 29, 2012
10.1021/nn204911k

potassium phthalic acid[4] or *N*-erucamidopropyl-*N*,*N*,-dimethylamine combined with maleic acid[5] have displayed the formation of pH-induced elongated wormlike micelles, which are interesting systems for their viscoelastic properties. Drug-delivery applications were also targeted in binary monolinolein/phloroglucinol systems,[6] but less importance was given to a specific study on the self-assembly mechanism. Furthemore, bolaform surfactants are also a large family of compounds that contain double hydrophilic units symmetrically located at each end of a hydrophobic spacer. Interesting pH-responsive aggregation properties have been observed on specific, well-designed molecules such as asymmetric bolaamphiphiles, but their laborious synthesis procedure may prevent a possible large-scale employment.[7−9]

In this context, a new, emerging field of biobased surfactants has been intensively studied in the past 20 years to fulfill the expectations of replacing nonrenewable, mineral oil-derived, products[10] in agreement with the 12 principles of green chemistry. Glycolipids are nonionic surface active agents composed of a hydrophilic carbohydrate-based head linked to a fatty acid or a fatty alcohol through an ester, an amide, or an ether bond.[11] They already replace, and/or are destined to massively replace, classical surfactant families like SDS or CTAB in home and personal care products. For these reasons, their physicochemical properties have been studied in the past 15 years. The effect of molecular structure (e.g., chain length, number of sugar units), concentration, use of cosolvents (short-chain alcohol, for instance), cosurfactants on the critical micelle concentration (cmc), surface tension, rheology, cleaning power, and self-assembly and mesophase formation have shown particular effects for many of these compounds.[11−13] These molecules are generally synthesized *via* several chemical strategies, reviewed by von Rybinski,[11] from renewable compounds like fatty acids and sugars. In terms of self-assembly, sugar-based surfactants show classical lyotropic behavior, as expected for ionic or nonionic compounds, but no specific stimulus-responsive property has been attributed to them until date. In addition, they are still much more expensive in their pure form with respect to classical surfactants; in fact, low-cost commercial alkylpolyglucosides (APG) are actually sold as formulations presenting either a nonconstant number of glucose units or mixtures of at least two different chain lengths. For these reasons, their use in nanoscience-related research topics has not been highly explored yet.

In a recent paper,[14] we have investigated the self-assembly and structuring properties of acidic sophorolipids (Figure 1), a family of entirely bioderived glycolipids. These natural compounds can be obtained in large amounts by yeast culture in the presence of several carbon sources, like glucose, fatty acids, and even alkanes and waxes.[15−18] Because of their reduced

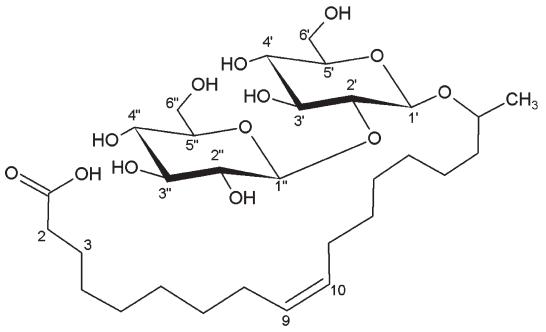

Figure 1. Acidic form of sophorolipids (SL) obtained from *Candida bombicola*.

environmental impact biosynthesis, confirmed by a recent life cycle analysis study,[19] sophorolipids (SL) have attracted the attention of the home- and skin-care industry.[20−22] Nevertheless, few recent studies have highlighted interesting anticancer[23] or self-assembly properties.[14,18] Nonetheless, the limited number of works involving SL has prevented a deeper knowledge and understanding of their physicochemical properties. Acidic SL are composed of a sophorose unit attached to an oleic acid moiety through an ether bond on the C17 carbon atom of the fatty acid chain. This particular feature leaves the COOH group unaffected in contrast with most fatty acid-derived surfactants obtained by chemical synthesis and in which the carboxylic group is generally engaged in an ester bond. Acidic SL are water-soluble, and the COOH group constitutes a good pH-responsive probe.

Zhou et al.[18] were the first ones to show the supramolecular assembling properties of SL in water supplying evidence of both pH and time factors. In our recent work,[14] we focused on the self-assembly of SL into different micellar objects (spherical, cylindrical, and wormlike), and we have shown how they can be exploited as porogenic agents in the synthesis of silica thin films. In this study, we provide more details on the behavior of SL in aqueous medium by demonstrating how their shape, long-range interactions, surface charge, and aggregate dimensions are governed by pH. In the domain of bioengineered glycolipids, rhamnolipids were also reported to have a pH-dependent behavior, their morphology changing from vesicles to micelles in the region $4.5 < pH < 7.0$.[24]

In a recent review on the self-assembly behavior of biosurfactants, Kitamoto et al.[25] focused on many compounds but sophorolipids were excluded. The study of simple, sustainable, bioderived, monocomponent, stimuli-responsive, and up-scalable molecular systems gives new perspectives in the scientific context described above. In addition, their close molecular similarity to specific nanotube-forming asymmetric bolaform surfactants obtained through chemical engineering suggests that their self-assembly behavior is up to now largely underevaluated.[26]

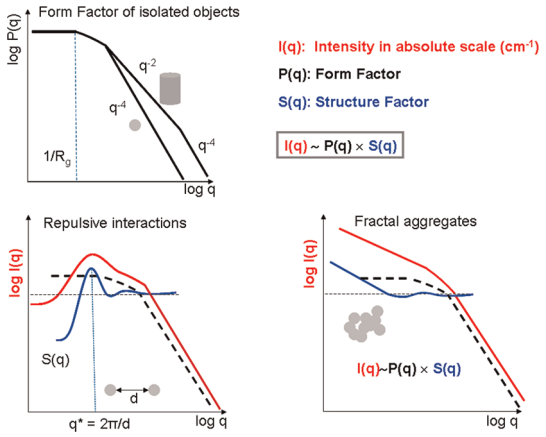

Figure 2. Schematic log−log representation of the typical neutron scattered intensity ($I(q)$) under diluted (isolated objects), interactive, and fractal regimes.

In this work, we propose a detailed study on the pH-responsive properties of the open acidic form of SL in water in the pH range between 4.5 and 11, corresponding to a degree of ionization,[27] α, between 0.2 and 1 at concentration values below 5 wt %. We show here, using a combination of small angle neutron scattering (SANS), cryo-TEM, and NMR experiments that variations in the degree of ionization of SL will introduce negative charges at the micellar surface inducing changes in their shape, aggregation state, and surface properties. In particular, SANS is a very powerful technique to study soft matter behavior in solution. Figure 2 shows a schematic representation of the main pieces of information that can be extracted from a log−log representation of a SANS spectrum. $I(q)$ is the scattered neutron intensity in absolute scale as a function of the wavevector q; $P(q)$ is the form factor and $S(q)$ the structure factor. For isolated objects, $S(q)$ is unitary and the analysis of slope of $I(q)$ (in log−log scale) provides information on the micellar shape. In the presence of repulsive interactions between well-defined objects, the structure factor cannot be neglected in the intermediate q-range, and it strongly contributes, generally with a scattering peak, to the overall $I(q)$, while it tends to a unitary value at high q. In the case of undefined shapes and sizes, as for fractal objects, one observes an undefined increase of the scattered intensity at low q values, whose slope, in some cases, can be related to the fractal dimension of the object.

In this particular study, SANS spectra clearly show the existence of at least three different regions where supramolecular SL aggregates are unexpectedly different. In contrast to many similar systems, whose rich nature of supramolecular assemblies is mostly driven by concentration effects above 5−10 wt %, we find here structures as different as nanometer-sized spherical micelles and large netlike aggregates of several hundred of nanometers can form when passing from $\alpha = 0.2$ to $\alpha = 1$.

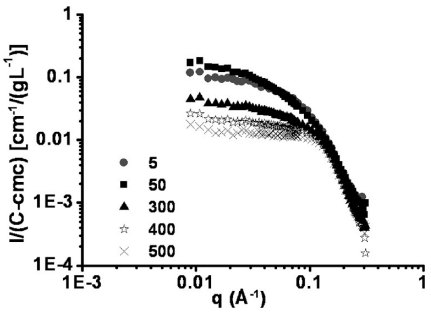

Figure 3. Log−log representation of $I(q)$ vs q of SANS experiments performed on SL/D_2O at different concentrations. Values are given in mg/mL. Intensity is concentration-scaled and normalized by the SL cmc. 4 < pH < 5.

RESULTS AND DISCUSSION

In a recent paper,[14] we have shown that at pH < 5 concentration of the acidic SL influences the shape of micellar geometry, going from spherical (5 mg/mL) to wormlike objects (220 mg/mL) in the self-assembly process. Additionally, we supply evidence of the fact that pH seems to have an effect on the long-range interactions between micelles at concentration values as low as 50 mg/mL. In the next sections, we will discuss in more detail the self-assembly behavior of SL as a function of pH.

Concentration Effects. In Figure 3, we show SANS experiments of SL in D_2O at 4 < pH < 5 as a function of SL concentration, which was increased up to 500 mg/mL. Data are normalized by the sample concentration, C, to which the cmc value of SL is subtracted in order to consider only the micellar contribution to the scattered signal. At low concentrations, $C = 5$ and 50 mg/mL, the signal can be fitted using the form factor, $P(q)$, of, respectively, a sphere and a cylinder, as schematized in Figure 2. With respect to our previous estimations,[14] different form factors can also be employed, as summarized in Table S1 in the Supporting Information. A better estimation of micellar size is given hereafter. At 5 mg/mL, a spherical or ellipsoidal model can be applied with typical radii around $R = 26.1$ Å for the sphere and $R = 15.4$ Å for the ellipsoid and a typical length of $L = 61.4$ Å for the latter. Polydispersity seems to play an important role for these systems, and values as high as 30% should be employed in order to fit the experimental data. At 50 mg/mL, the cylindrical model is by far the best suited where $R = 14.2$ Å and $L = 139.0$ Å with a polydispersity of 18%. A vesicle form factor can also be used but the polydispersity increases up to 50%, which does not seem to be a reasonable value. The corresponding fits are given in Figure S1 in the Supporting Information.

When the concentration is increased up to 500 mg/mL, a decrease in the absolute intensity at low q values occurs, as expected for more condensed matter. At the same time, a very weak and broad interaction peak is detected at approximately $q = 8.10^{-2}$ Å^{-1}, corresponding

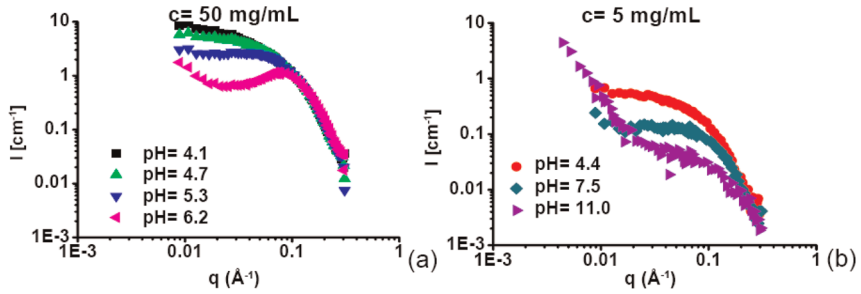

Figure 4. log−log representation of $I(q)$ for SL solutions at (a) 50 mg/mL and (b) 5 mg/mL at increasing pH values.

to an intermicellar distance, d, of about 70 Å: a nonunitary structure factor, $S(q)$, contributes then to $I(q)$, as also schematized in Figure 2. At this concentration, micelles are most likely constituted of entangled wormlike objects,[14] but if one considers that the measured cross-section of the cylinders is approximately 30 Å, it can be deduced that they are not in direct contact, but rather with an average micelle-to-micelle distance of the order of 40 Å. Despite the relatively high SL concentration in solution, repulsive long-range intermicellar interactions do not seem to play a major role.

pH Effects. The role of pH on the self-assembly of SL in solution was briefly shown by Zhuo et al.[18] Using optical microscopy and FT-IR arguments, they reported the formation of short-range interacting micelles at pH = 7.8 and, for concentrations above 1 mg/mL, the formation of large aggregates (radius of gyration, R_g > 100 nm). Nevertheless, these techniques are less adapted to characterization of nanometer-scale systems with respect to small angle scattering techniques. In our previous work, SANS experiments demonstrate that long-range micellar interactions can develop as a function of pH at a given concentration, but no details were given about the nature of these interactions. Hereafter, we go deeper in the understanding of these phenomena. In Figure 4a,b we report the log−log evolution of SANS intensity recorded on SL solutions at different pH values for two concentrations: 50 mg/mL (5 wt %) (Figure 4a) and 5 mg/mL (0.5 wt %) (Figure 4b). The differences among the low-angle scattering curves allow us to identify at least three different regimes.

Regime 1 (pH < 5). Increase in concentration drives micellar shape from spherical (red circles) to cylinders (black squares) to wormlike (see ref 14).

Regime 2 (5 < pH < 8). The effect of pH on self-assembly in this pH range is reflected on the long-range micellar interactions. A broad, but strong interaction peak grows in the 50 mg/mL system due to a nonunitary structure factor, $S(q)$ (Figure 4a), as also schematized in Figure 2. The spectrum at pH = 6.2 is also followed by an increase in intensity at low q values. Both phenomena, to a lesser extent, are also observed on the 5 mg/mL solution at pH = 7.5 (Figure 4b).

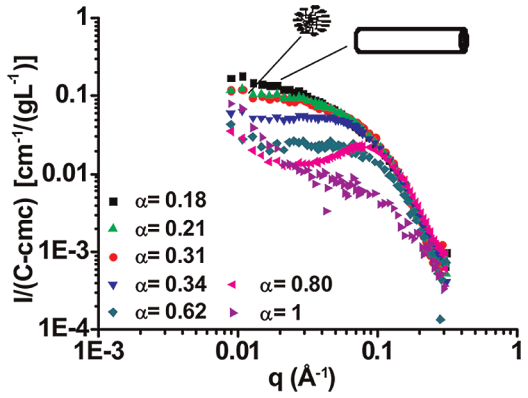

Figure 5. Concentration and cmc-scaled data presented in Figure 4 as a function of the ionization degree, α, calculated according to eq 1. Details about the fits and derived micellar geometrical data can be found in Figures S1 and S2 and Table S1 in the Supporting Information and Table 1.

Regime 3 (pH> 8). Higher pH values seem to provoke a disruption of intermicellar interactions, as shown by the loss of the characteristic peak in the 5 mg/mL system (Figure 4b) at pH = 11.0. On the contrary, a very strong increase in $I(q)$ occurs at q < 0.03 Å^{-1} indicating the existence of large aggregates, whose interesting nature will be described later.

If compared to nonionic glycolipids, SL have unexpected features; their pH-responsive behavior derives from the free COOH group and its degree of ionization, which plays a major role in the overall self-assembling properties. The amount of residual COO^- in SL upon increasing pH can be estimated by adding the fraction of self-dissociated COOH at equilibrium, $[COO^-]_{sd}$ (sd stands for self-dissociation). The former can be estimated by the dissociation constant of oleic acid (pK_a of oleic acid is 4.8[28,29]) in water and after determining its equilibrium pH, and the amount of added sodium hydroxyde, used to neutralize the carboxylic acid groups. The concentration of COO^-, $[COO^-]_{NaOH}$, is then directly proportional to the molar concentration of NaOH. In this case, it is interesting to consider the overall degree of ionization, α, defined in eq 1:

$$\alpha = \frac{[COO^-]_{sd} + [COO^-]_{NaOH}}{[COOH]_{SL}} \quad (1)$$

From now on, we will refer to all experiments in terms of the SL ionization degree and spectra presented

TABLE 1. Results from Fits of SANS Data Shown in Figure S1 (α = 0.31; α = 0.18) and Figure S2 in the Supporting Information

C (mg/mL)	α	form factor	R (Å)	σ	L (Å)
5	0.31	sphere	26.1	0.30	
		ellipsoid	15.4	0.21	61.4
	1	sphere	16.0	0.30	
50	0.18	cylinder	14.2	0.18	139.0
	0.21	sphere	30.7	0.40	
		ellipsoid	15.0	0.29	77.4

in Figure 4a,b can be normalized with respect to the SL concentration (5 and 50 mg/mL), as shown in Figure 5. Please note that, even if now data can be discussed as a function of α, which is done afterward, unexpected effects due to concentration may occur and a systematic study is eventually needed. Hereafter we rather focus on a new, phenomenological, self-assembling behavior to which sophorolipids are submitted under the selected conditions.

Data presented in Figure 5 suggest that α strongly drives the self-assembly of SL from regime 1 through regime 3 with limited influence on concentration, at least for the tested values. At α > 0.3, a transition occurs between regime 1 and 2 while one has to reach at least α = 1 to be in regime 3.

Table 1 shows the values of the fits of SANS data for SL solutions at C = 5 mg/mL and 50 mg/mL at different α values. Interestingly, for the 50 mg/mL system, when α increases from 0.18 to 0.21, spherical (R = 26.1 Å) or ellipsoidal (R = 15.0 Å; L = 77.4 Å) geometry models must be employed instead of the cylindrical one. The same models must be used to fit the lower concentration system, C = 5 mg/mL, where micelles are spherical up to α = 0.31. At α =1, fit of the full data set becomes challenging but an estimation of the micellar cross-section can be done by fitting only the high-q data region. A sphere form factor can be employed, as shown in Figure S2 in the Supporting Information, providing R = 16.0 Å (Table 1). Nevertheless, a specific insight on the nature of the aggregates obtained at α = 1 conditions will be given later.

The shape of SL micelles is highly influenced by the pH, and the above data show that, at a given concentration and increasing ionization degree, the micellar curvature increases because of a cylinder to ellipsoid/sphere transition, as shown by comparing, at 50 mg/mL, the system at α = 0.18 and α = 0.21. In addition, as expected, the size of the SL micelle increases when passing from the low to high concentration system (Table 1). In the spherical model hypothesis, the radius goes from 26.1 Å (5 mg/mL) to 30.7 Å (50 mg/mL), while in the ellipsoid model, the radius is practically constant (R = 15.0 Å) but the length varies from 61.4 Å (5 mg/mL) to 77.4 Å (50 mg/mL). When decreasing the value of α at 50 mg/mL, the length of the cylinder goes from 77.4 Å to 139.0 Å.

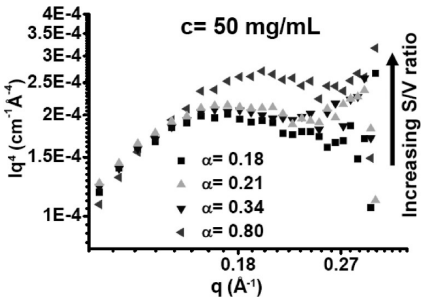

Figure 6. Porod plot [$I \cdot q^4(q)$] of SL solutions at 50 mg/mL at four different values of α. S/V stands for surface-to-volume ratio.

These data will be discussed in depth in the following text, but one can state that SL have interesting pH-responsive self-assembling properties in water. Nevertheless, many questions are still open, in particular regarding the nature of the interacting aggregates in regimes 2 and 3.

SL Behavior in Regime 2. At a concentration of 50 mg/mL (α = 0.18), SL form cylindrical micelles, as discussed previously. Hereafter, we try to elucidate the evolution of the cylindrical shape as a function of the degree of ionization at this same concentration. This analysis will provide valuable pieces of information concerning the overall nature of SL aggregates. The Porod region at high q values of the SANS spectra is of extreme importance because it allows us to compare the overall surface-to-volume ratio (S/V) of the scattering objects independently from the value of the structure factor, $S(q)$ ($\lim_{q\to\infty} S(q) = 1$). This is done by plotting Iq^4 as a function of the wavevector, q. At high q, the Iq^4 value extrapolated at q = 0, the Porod plateau, is directly proportional to S/V. Since, from simple geometrical considerations, S/V is bigger for a sphere than for a cylinder, one can expect that, in a qualitative way, a cylindrical or wormlike micellar system should have low $Iq^4(q = 0)$ values. Figure 6 represents the variation of Iq^4 as a function of q for C = 50 mg/mL, for various degrees of ionization. In general, the Porod law is dependent on the volume fraction, ϕ, which, in this case, is strictly equal for all samples allowing a straightforward comparison among the spectra (here, ϕ = 5.2 vol %). At α = 0.18, micelles are known to be cylindrical objects whose length ranges between 130 and 160 Å (aspect ratio around 5), as described after Figure 3; at higher ionization degrees, α = 0.21 and α = 0.34, the Iq^4 curves display a slight increase at q = 0, but they are still very close to the one at α = 0.18. On the contrary, at α = 0.80, the Iq^4 plateau, whose value ($Iq^4 = 2.7 \times 10^{-4}$ cm$^{-1}\cdot$Å^{-4}) is about 30% higher than the corresponding value for the α = 0.18 system ($Iq^4 = 1.9 \times 10^{-4}$ cm$^{-1}\cdot$Å^{-4}), suggests an increment in S/V: the overall micellar surface increases. This phenomenon, in contrast with the expected evolution of SL micelles toward branched wormlike systems, can be interpreted with a shortening of the micellar length.

Interestingly, after simple geometrical considerations, the relative gain in the calculated S/V for a rod-to-sphere transition is about 33%, and a similar behavior can be found in the α-driven cylinder-to-sphere transition in PS-PAA systems.[30] The experimental representation of the structure factor, $S(q)$, calculated for the same data set (details can be found in Figure S3 and related discussion in the Supporting Information) confirms the overall change of micellar shape going from $\alpha = 0.18$ to $\alpha = 0.80$.

As a general comment on the presence of a structure factor (one can also refer to scheme on repulsive interactions in Figure 2), one should remember that in many systems a minimum 5−10 wt % surfactant concentration has to be reached in order to observe a prominent interaction peak, related to long-range repulsive interactions, but this value can increase up to 20 wt %.[31−38] Furthermore, in the specific case of alkylpolyglucosides (APG), no pH-driven long-range ordering of micelles is found until concentration values reach at least 10−20 wt %.[12,39−41] On the contrary, long-range intermicellar interactions for these systems can be controlled at lower concentrations by adding specific electrical charges at the micellar outer surface using ionic surfactants.[42] In SL-based systems, electrical charges are autogenerated by pH (deprotonation of COOH group).

Local analysis using transmission electron microscopy under cryogenic conditions is performed on the $\alpha = 0.80$ sample and shown in Figure 7a,b agree with the Porod plot analysis. The sample is constituted of spherical micelles, specifically indicated by the arrows in Figure 7b. The average cross-section radius (R_m) and its size distribution are shown in Figure 7c, and they correspond to $R_m = 21.9$ Å with $\sigma = 2.2$ Å. Larger micelles ($R_m > 60$ Å and $L > 100$ Å), which could actually explain the increasing $I(q)$ in SANS at low q in Figure 5 are also found in cryo-TEM images.

Finally, combination of these techniques provides an answer to interpret the nature of the interaction peak observed in Figure 5 for $\alpha = 0.80$. In regime 2, in close proximity to neutral pH, SL micelles undergo a rod-to-sphere transition where long-range interactions, but not long-range order (at least not at 50 mg/mL), appear.

SL Behavior in Regime 3. At higher COO^- concentration, the interaction peak in the mid-q region is not detected anymore (Figure 4b, $\alpha = 1$), while the scattered intensity at low q increases without reaching a plateau. Figure 8 focuses on the SANS experiments performed on two samples at $C = 5$ mg/mL, both at $\alpha = 1$, but at different NaOH concentration. First, spectra can be superimposed in the whole q range indicating no apparent influence of the amount of sodium hydroxide at $\alpha = 1$. The discussion next will be focused on the system at [NaOH] = 12.5 mM, corresponding to pH = 11. Please remark that a slight excess of base with respect to the full ionized COO^- might be required to achieve this specific regime.

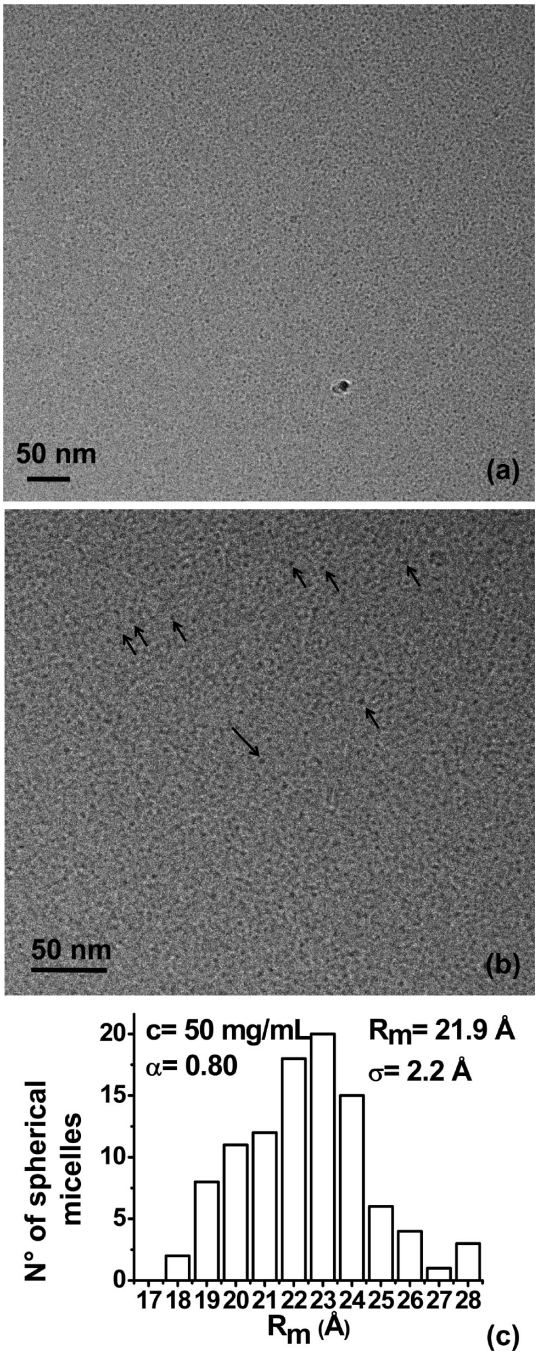

Figure 7. (a, b) High-resolution (magnification: ×80k) cryo-TEM experiments performed on SL-sample at $C = 50$ mg/mL and $\alpha = 0.80$. The darker spherical objects represent the SL micelles frozen in a thin layer of amorphous ice. Images are corrected for the camera noise. (c) Size distribution of the cross-section micellar radius (R_m) related to spherical micelles observed in (a, b).

Second, the signal-to-noise ratio of $I(q)$ throughout the whole q range is poor, if compared to the same system ($C = 5$ mg/mL) at $\alpha = 0.31$ (Figure 4b), meaning that the lower concentration value is not responsible for such loss in signal intensity. Due to the poor quality

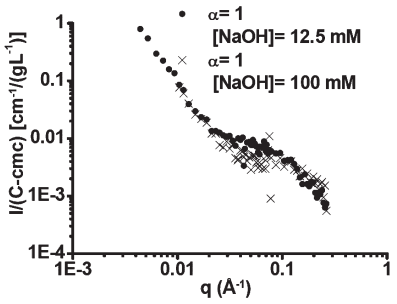

Figure 8. SANS experiments performed on two SL solutions at α = 1 but different NaOH concentrations. Data on the [NaOH] = 12.5 mM (pH = 11) system (full circles) were completed with ultralow angle experiments ($q < 8.38.10^{-3}$ Å^{-1}) to confirm the increase of $I(q)$.

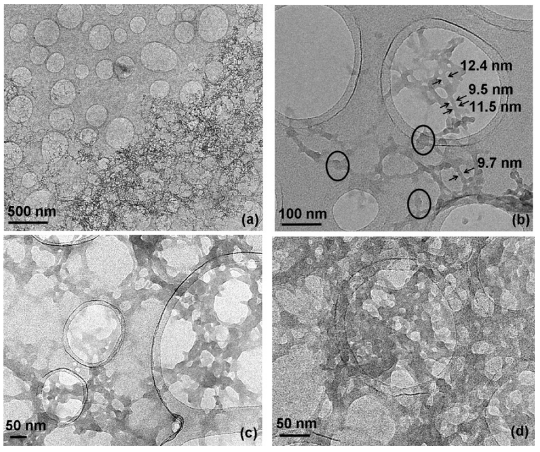

Figure 9. Cryo-TEM images performed on the SL solution at α = 1 and [NaOH] = 12.5 mM. Note that the gray homogeneous background is the classical amorphous holey carbon layer on top of the TEM copper grid while the circular shapes indicate the amorphous-ice covered holes within the membrane.

of SANS data, we prefer not to pursue a detailed discussion based on the classical analysis of the log[$I(q)$] *vs*. log[q] slopes. A fit of the high-q region using a sphere form factor provides a gross estimation of the micellar cross-section ($R = 16$ Å), as shown in Figure S2 in the Supporting Information.

On the contrary, the very strong increase in $I(q)$ at low q values (8.38×10^{-3} Å$^{-1} < q < 7.32 \times 10^{-2}$ Å^{-1}), confirmed by additional experiments at very low q ($q < 8.38 \times 10^{-3}$ Å^{-1}) for the [NaOH] = 12.5 mM system (full circles in Figure 8a), give a strong hint of the existence of large micellar ($R > 50$ nm) structures whose size and shape cannot be determined by SANS (for a better understanding, one can refer to the schematic representation of fractal geometries in Figure 2). The diffuse q behavior and very low intensity above 0.02 Å^{-1}, which could indicate unstable micellar objects and interfaces, is more difficult to explain. Similar data were reported by Zhang et al.,[39] who also experienced diffuse high-q scattering in alkylglucoside solutions and attributed it to large fluctuations in the position of molecules within the micelles which depends on the less marked hydrophilic/hydrophobic character of these surfactants. In a slightly different system, Bendejacq et al.[30] have shown a swelling effect of COOH brushes in PS-PAA copolymers at increasing α. Here, it can be symptomatic of both a less stable interface and a reduction in the amount of small-sized micelles, otherwise abundant at lower α-values.

To complete SANS experiments and better explain the nature of the aggregates, we performed transmission electron microscopy under cryogenic conditions on the sample at α = 1 and [NaOH] = 12.5 mM, (Figure 9a–d). The amount of individual micelles seems to be far less important with respect to systems studied in Figure 7; most attempts to observe them inside the amorphous ice holes were unfruitful, but the low-intensity signal at high q in SANS, as shown by the fits in Figure S2 in the Supporting Information, cannot completely exclude their presence. On the contrary, we could observe separate regions composed of a dense system of elongated, branched aggregates, as shown in the overview image in Figure 9a. A close look at the micellar region shows an ill-defined system composed of interconnected tubules whose average side diameter is about 13 ± 3 nm (see arrows in Figure 9b). The overall dimensions of the clusters comprise between 100 and 500 nm, and the unorganized network identifies hollow cavities whose size ranges between few nanometers to 100 nm. Individual branches of much smaller size or long (>100 nm) flexible objects are also observed (Figure 9b,c). The exact description of the supramolecular aggregates formed under high pH conditions is a difficult task as well as the explantion of their origin. We could not easily find in the literature a similar surfactant system with such a different behavior as a function of pH. Nevertheless, several synthetic asymmetric bola-form surfactants have been reported to form nanotubes, generally referred to as lipid nanotubes.[43] In these works, individual nanotubes were clearly identified, and random aggregation, similar to what it is observed here, does not occur as much. For one particular surfactant, whose molecular structure is close to the one of sophorolipids, well-defined nanotubes are obtained under acidic conditions, but more globular, ill-defined structures were reported at higher pH values.[26] Unfortunately, the authors did not further investigate the influence of high pH on the supramolecular assembly of their compounds. In the SL-based system obtained under basic conditions we could seldom observe isolated elongated aggregates, and in any case, they cannot be closely related to well-defined nanotubular objects. On the contrary, as one can observe in Figure 9b (black circles), where these structures could be isolated, they are composed of an elongated tubular scaffold with local hemispherical, vesicle-like protuberances. An interesting tubular-to-vesicle transition as a function of temperature

was described by Imae *et al.*[44] during the study of a fluorinated−hydrogenated glucophospholipid. They attributed such a phenomenon to a local molecular variation of the surfactant packing. The average side diameter of our tubules is comparable with the one reported by several authors on lipidic nanotubes.[26,44] In particular, Masuda and Shimizu[26] were able to correlate the stacking periodicity and the size of the inner tube diameter with the chain length and packing of their bolaamphiphiles. In our system, sophorolipids have a C18 chain, which according to the model proposed by Masuda and Shimizu and in the case that it could be applied to this specific system, should provide tubules whose diameter ranges between 18 and 20 nm. The average side diameter observed here (13 ± 3 nm) is slightly smaller, but one should probably consider the influence of the SL C=C double bond on the local molecular packing.

SL Molecular Configuration. The degree of ionization introduces negative charges determining, at mild α values, electrostatic repulsive forces with a strong influence on both the shape and size of the aggregates. An important issue is the local conformation of the SL molecule and, in particular, the localization of the COOH/COO^- group within the micelle as a function of α. Upon neutralization, one can also reasonably suppose that COO^- groups move toward the external micellar surface, being responsible for their negative charge. ζ-potential, ζ, experiments are useful to determine in a qualitative way the charge at the micellar surface. For instance, at $C = 5$ mg/mL, the following values for ζ-potential, $\zeta = -29.7$ mV and $\zeta = -49.1$ mV, were measured, respectively, for the $\alpha = 0.31$ and $\alpha = 0.62$ systems, while at $C = 50$ mg/mL, ζ varies between -10.0 mV and -25.0 mV for $0.2 < \alpha < 0.8$. As expected, in all cases the micelles show a negative surface charge, whose absolute value seems to increase with α at a given concentration. Local electrostatic repulsions between COO^- groups may also account for the increase in the micellar curvature at $C = 50$ mg/mL, going from cylinders to spheroids when α shifts from 0.18 to 0.80, as discussed previously.

To draw a picture of the local molecular conformation of SL within the micelles, we ran a set of $^1H-^1H$ two-dimensional nuclear Overhauser enhancement spectroscopy (2D NOESY) NMR experiments on three SL solutions at variable α values, each corresponding to a specific regime. 2D NOESY NMR is an effective method to study the three-dimensional structure of large molecules that have a long motional correlation time, such as proteins.[45,46] This type of 2D spectrum displays NOE cross-peaks located at the chemical shift of protons that are correlated through magnetization transfer mediated by dipole−dipole interactions. The effect occurs through space and is independent of covalent bonds. It is strongly distance-dependent, and protons normally need to be separated by less than 5 Å to be observed in NOESY spectra. Cross-signals in a NOESY spectrum rely on the cross-relaxation of longitudinal magnetization during a selected mixing time. 2D NOESY is currently employed to characterize internuclear distances and molecular conformation in surfactants micellar systems[47,48] and it will be employed here to probe proton−proton proximities within SL; in particular, we will focus on the interactions involving the COOH group.

$^1H-^1H$ 2D NOESY experiments (Figure 10 a,b) were run on solutions at $\alpha = 0.18$, $\alpha = 0.80$ ($C = 50$ mg/mL), and $\alpha = 1$ ($C = 5$ mg/mL; [NaOH] = 12.5 mM), while mixing time, $\tau_m = 300$ ms, was selected on the basis of a build-up curve run for 50 ms $< \tau_m <$ 900 ms, typical values used in the study of surfactant-based systems in water above their cmc value (the acidic SL has $cmc_{SL\text{-}COOH} = 0.11$ mg/mL while its cmc after deprotonation is $cmc_{SL\text{-}COO^-} = 0.15$ mg/mL. Refer to Sample Preparation and Figure S4 in the Supporting Information for more details on cmc data of SL). The ^1H chemical shift attribution is done on the basis of the 1D spectrum (top of the 2D NOESY maps and scheme in Figure 10c):[17] (1) oleic acid moiety: H_2 ($HOOCC\underline{H}_2CH_2-$) at 2.15 ppm; H_3 ($HOOCCH_2C\underline{H}_2-$) at 1.51 ppm; $H_{9,10}$ ($-\underline{H}C{=}C\underline{H}-$) at 5.30 ppm. 2) Sophorose moiety: $H_{1'}$, $H_{1''}$ (anomeric $-OC\underline{H}O-$) at 4.45 ppm; $H_{(2-6)'}$, $H_{(2-6)''}$ ($-OC\underline{H}-$) at 3.16−3.8 ppm.

The H_3 signal, in close proximity to the carboxylic acid, is good for interactions between the end of the oleic acid (OA) chain and the sophorose headgroup. The NOESY response of the sample at $\alpha = 0.18$ (Figure 10a) shows several cross-peaks, highlighted in gray in the F1-dimension and connected through the black lines, related to the H_3 carbon signal. Dotted lines identify close neighbor connections between H_3 with the oleic acid backbone ($\delta = 1.26$ ppm) and H_2, while solid lines identify several interesting long-range connections with $H_{9,10}$ and sophorolipid head ($H_{1'}$, $H_{1''}$, $H_{(2-6)'}$, $H_{(2-6)''}$). For comparison, at $\alpha = 0.80$ and at equal mixing times (Figure 10b), short-range interactions like H_3-H_2 are still detected, as expected, while the long-range connections with sophorose are almost completely lost. At $\alpha = 1$ (map not shown), no cross-peaks at all are detected, except for those relating to close neighbors interactions. In Figure 10d, we compare, as a function of α, the slices extracted from the 2D NOESY map at $\tau_m = 300$ ms, corresponding to the H_3 resonance ($\delta = 1.51$ ppm; refer to the solid arrow in Figure 10): the intensity of the corresponding H_3-sophorose cross-peaks decreases with α. A similar trend was observed at lower mixing times ($\tau_m = 50$ ms), at which $^1H-^1H$ spin diffusion artifacts may considered to be minimized.

NOESY experiments qualitatively show that the COOH environment of oleic acid backbone is in close interaction with the sophorose moiety at low α, while this is not the case at higher ionization degrees.

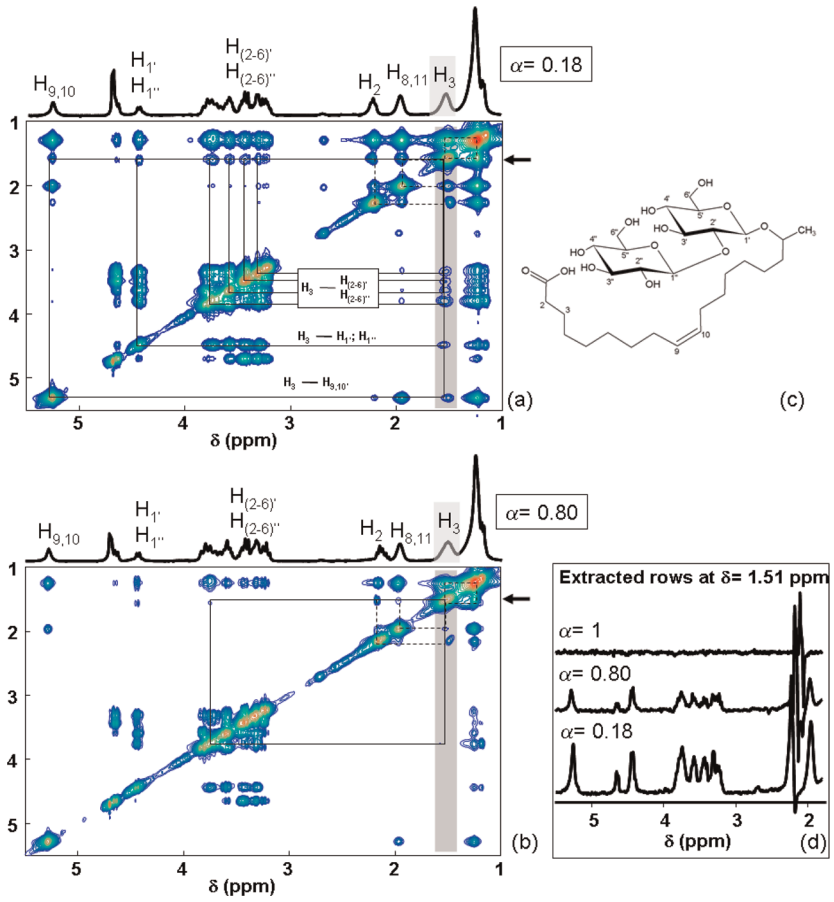

Figure 10. $^1H-^1H$ 2D NOESY NMR experiments performed at a mixing time of 300 ms for SL solution at $C = 50$ mg/mL at (a) $\alpha = 0.18$ and (b) $\alpha = 0.80$. (c) SL molecule with typical convention for ^1H chemical shift assignment. (d) Comparison of extracted rows at $\delta_{1H} = 1.51$ ppm (black arrow) from the corresponding 2D NOESY experiments. Note that both samples are prepared at the same concentration and 2D NOESY spectra are acquired using the same NMR parameters and, most importantly, postacquisition treatment (e.g., contour plot height).

Strong hydrogen bonds between COOH and OH groups in sophorose may explain this behavior even if it is impossible to discriminate between interactions occurring within the same or between two adjacent SL molecules. In the field of bolaform surfactants having an all-*trans* conformation of the aliphatic chain, adjacent molecules are proposed to be either in a parallel or an antiparallel configuration,[26,49] as also shown in Figure 11. In this case, NOESY experiments could help probing interactions in close spatial environments and one could probably discriminate between them. Unfortunately, if folding of the alkyl chain occurs, as it could be the case for sophorolipids (one should not forget that SL are mostly produced in their close lactone form and are characterized by a *cis*- C═C double bond), clear-cut discrimination through NOESY NMR experiments becomes highly challenging, if not impossible. In this case, one would expect the same spatial proximities in both the parallel and antiparallel configurations, as sketched by the pointed lines in Figure 11 (*cis* configuration).

In the $\alpha = 1$ system, one can observe the absence of long-range intermolecular interactions, which is partly unexpected even if that confirms the absence of large amounts of small micellar objects. Yet, it is not excluded that the diffusion dynamics of the large aggregates observed in cryo-TEM are too slow and their transverse relaxation time too small to be observed under the actual conditions; the signal for this particular system may actually corresponds to free SL molecules. Further experiments are ongoing to verify this hypothesis. To account for these observations one can formulate the hypothesis that the large micellar aggregates contain mobile SL molecules, probably forming a monomolecular layer, which are solvated with large amount of water, both inside and outside the tubular structures, implicitly suggesting a hollow tubular configuration, as often reported for related systems.[26,50]

Overview on SL Conformation and Self-Assembly. The molecular structure of SL resembles the one of glycolipids but COOH group has an important impact on the self-assembly process and the stability of micelles as a function of pH and time. Unfortunately, most studies on natural surfactants were done on classical glycolipids, and no specific term of comparison involving SL is available at the moment. The theoretical micellar

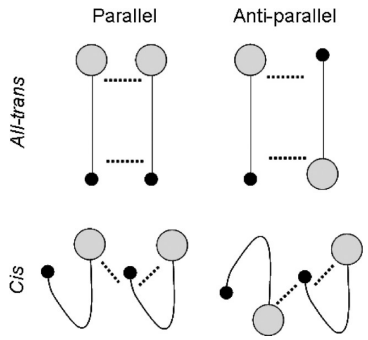

Figure 11. Scheme of the possible parallel and antiparallel configurations of bolaform surfactants in the case of an *all-trans* configuration of the alkyl chain, as proposed in ref 26, and in the presence of a *cis* C═C double bond as it occurs in sophorolipids. Dotted lines represent close-rage through-space interactions.

radius of a fully elongated SL molecule, corresponding to a β-anomer conformation, should include the contribution of oleic acid (OA) (approximately 22 Å[51,52]) and sophorose, whose size can be estimated to be below 10 Å. This value is obtained by comparison with *N*-dodecyl-β-maltoside ($C_{12}G_2$), in which, according to experimental and modeled data, maltose (a common disaccharide comparable to sophorose) does not contribute to more than 6 Å to the size of $C_{12}G_2$ in its linear conformation (β-anomer).[53]

Under these conditions, one expects a cross-sectional radius for SL micelles of approximately 30 Å. In reality, the experimental data measured by SANS are 30% to 50% lower depending on the micellar shape (sphere, ellipsoid, or cylinder) in the low ionization degree regime, as discussed before and shown in Table 1. These discrepancies are too large to be neglected. Typical cross-sectional radius reported in literature for sodium oleate micelles is 26 Å[54] while for an oleic-acid based glycolipid, whose polar head is constituted by a disaccharide and referred to as OM,[40,55] is 25 Å. It is very interesting to note that almost no discrepancy exists between the cross-section sizes of sodium oleate and OM, despite the additional disaccharide group in the last compound. As shown by Abel et al.[53] for $C_{12}G_2$, this can strongly depend on the α (right angle bending between the sugar and tail) or β anomeric configuration of the disaccharide with respect to the aliphatic chain. The same authors have also outlined the importance of the strong hydrogen bonding in which the maltose head is involved and that 10% of the hydrophobic chain is permeable to water. The cross-sectional radius measured by SANS for SL spherical micelles (5 mg/mL, α = 0.31) is 26.1 Å, which suggests that the sophorose group acquires a α-anomer conformation. Nevertheless, this is in contrast with previous works in which β-conformation was reported for SL.[17,56] As a first conclusion, one can then say that the OA moiety probably does not acquire a fully elongated conformation. When a sphere-to-cylinder transition occurs or when an ellipsoid form factor is used, the cross-sectional radius determined by SANS is even smaller (about 15 Å). Cross sections for cylindrical micelles are reported to be equal or even slightly smaller (<10%) than the corresponding spherical systems in many spheres for systems ranging from classical surfactants like CTAB[33] to glucose based compounds.[39,40] Nevertheless, a 40% difference as observed in SL is too large to be explained by chain conformation, packing or curvature differences, as usually done.

NOESY experiments above may provide an explanation to these discrepancies. The folding of the OA moiety, which was described before for SL,[56] can be driven by hydrogen-bond interactions between the COOH group and the sophorose, either within the same or, most likely, between two adjacent SL molecules. In this case, the effective length of the SL molecule and, consequently, of the micellar radius is smaller, especially if sophorolipids molecules are parallel to each other and the oleic acid backbone is folded, as shown in Figure 11 (*cis* configuration). Nevertheless, one should also consider the possibility of an antiparallel configuration (Figure 11), as also proposed in ref 26 for bolaform surfactants and discussed above. Further experiments and structural modeling are needed to confirm this assumption. At a higher ionization degree, the COO^- has weaker interactions with sophorose and its hydration degree is probably higher, which may induce a non-negligible water intrusion at the micelle/solvent palisade and, eventually, within the micellar core. Under these conditions we expect an increase in the micellar radius, which seems to be confirmed by cryo-TEM analysis in Figure 7 indicating an average 21.9 Å radius for the 50 mg/mL system at α = 0.80. At even higher α, the overall ionization effect on the structure of SL and the corresponding effect on the overall aggregate size, morphology and cross-section is not very clear, yet. Larger micellar aggregates are identified by the combination of SANS and cryo-TEM but the lack of any cross-peaks in 2D NOESY NMR experiments could reveal a strong SL mobility and an unstable micellar interface, probably integrating bigger amounts of water within the large tubules shown by cryo-TEM experiments. ^{1}H 1D NMR experiments (results not shown) may corroborate this hypothesis: the ^{1}H NMR signal corresponding to the H_2 group of SL for α = 1 is systematically narrower than at lower α and its chemical shift is slightly deshielded. This last feature is also observed for free oleate molecules below their critical micelle concentration.[57] In any case, under these conditions, the antiparallel arrangement of two adjacent SL molecules is a hypothesis to be considered with good probability where the free COO^- group would be solvated by water both inside and outside the tubule. Whatever the configuration adopted by adjacent SL molecules, the micellar surface becomes negatively charged with pH.

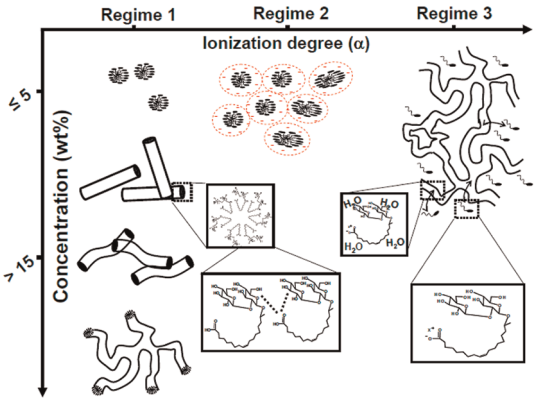

Scheme 1. Schematic Overview of SL Self-Assembly in D_2O as a Function of Concentration and Ionization Degree within 24 h of Preparation of the Solution. Note that drawings are not scaled.

Scheme 1 provides a schematic overview over the possible α-driven micellar regimes of SL in water described above. Please note that adjacent SL molecules are presented in a parallel configuration but one should not exclude, especially at high ionization degree, the possibility of an antiparallel form, as proposed elsewhere,[26] and discussed above.

Low α: micelles form above the cmc and their shape evolves from spherical to wormlike (curvature decreases). The micellar surface is mostly neutral and excluded volume drives intermicellar interactions, in which electrostatic effects do not play a major role. The behavior of SL in this regime is similar to classical glycolipid-based surfactants. Locally, the COOH groups seem to interact through hydrogen bonding with the sophorose moiety. Entanglement of adjacent oleic acid chains cannot be excluded. Such a hydrogen bonding configuration is explicitly shown in Scheme 1.

Intermediate α: deprotonation of COOH into COO^- introduces electrical charges located at the surface of the micellar objects. Micellar shape is strongly affected since its curvature increases: at a given concentration, a rod-to-sphere transition is observed and a mixture of spherical and obloidal micelles is largely observed. The introduction of electrostatic intermicellar repulsive effects result in long-range interactions at concentration values as low as 50 mg/mL. The effect of concentration at intermediate α was not studied here.

α = 1: when all COOH turn into COO^- and in probable excess of added base, the shape and size of micelles is drastically affected: very long (>100 nm) tubules (diameter >10 nm) entangle together to form micellar aggregates of ill-defined shape and surrounding water-rich gaps. The amount of free micelles is largely reduced according to high-q SANS and cryo-TEM arguments while solvation of SL molecules by water within the large aggregates is not excluded. The hydrophilic/hydrophobic balance of SL is drastically reduced causing a higher SL solubility and rapid disruption of the micelle/water interface. The exact nature and composition of these aggregates and the local conformation of SL in this regime needs further studies to be better understood.

CONCLUSION

In this work, we have investigated the self-assembly properties of acidic sophorolipids (SL), a bioderived glycolipid containing a free COOH group, as a function of the degree of ionization of its internal COOH group. SL are biosurfactants with a very low cmc and form, under acidic conditions, spherical, cylindrical, and wormlike micelles as a function of concentration. Above 300 mg/mL, the micellar entanglement strongly increases but SANS experiments show that long-range interactions are not directed by electrostatic repulsive forces, as it usually occurs for ionic surfactants, but by the higher volume fraction occupied by the compound. This behavior, which is identified in this study as regime 1, is very close to many other sugar-derived surfactants and it depends on the nonionic nature of these compounds. On the contrary, slight increase in pH induces the ionization of the COOH group, and the consequent increase in the ionization degree, α. At $\alpha < 1$, the nature of intermicellar interactions drastically change and regime 2 starts: two phenomena occur at the same time: (1) micelles undergo a low-to-high curvature transition (cylinder-to-sphere/ellipsoid) due to the introduction of negative charges at their surface; (2) electrostatic repulsive forces drive long-range interactions between micellar objects, as observed both by SANS and nicely confirmed by cryo-TEM microcopy. Interestingly, SL behavior in regime 1 and 2 clearly indicates that one can tune, for a given shape, the properties of micellar surface, from neutral to negatively charged, making these objects very versatile for a number of applications in nanoscience related fields. At $\alpha = 1$ (5 mg/mL) a new, unexpected, state of SL supramolecular assemblies occurs. In regime 3, all SL molecules are negatively charged and their hydrophilic/hydrophobic character is less pronounced. The micelle/water interface seems to be disrupted (SANS behavior at high *q*) and the presence of monomers is now favored (as also seen by ^1H NMR); nevertheless, SANS experiments agree on the existence of very long (>100 nm) micellar tubular (average diameter is 13 nm) aggregates organized in a net-like structure of ill-defined shape, as also shown by cryo-TEM experiments. The true SL behavior in this regime needs still to be clarified. At a local scale, NOESY experiments suggest that intra/intermolecular COOH-sophorose hydrogen bonding characterizes the low α regime but they do not bring any clarification on the local SL parallel or antiparallel configuration.

These experiments show that sophorolipids constitute an extremely versatile micellar system whose pH-driven properties make them an interesting stimuli-responsive

compound at very low concentration values (<5 wt %), which is quite atypical for comparable surfactant-based systems. The three different regimes, neutral and charged micelles at low-medium degree of ionization followed by large netlike aggregates at high α clearly show the potential versatility of these molecules.

EXPERIMENTAL SECTION

Synthesis of SL. Sophorolipids were produced by *Candida bombicola* (teleomorph: *Starmerella bombicola*) ATCC 22214. The yeast was cultivated on medium as described previously.[58] A fed-batch fermentation was run in a Biostat B culture vessel (Sartorius-BBI Systems) with a maximum working volume of 1.5 L. Temperature (30 °C), pH (3.5), stirring rate (800 rpm) and airflow rate (1 vvm) were controlled by the Biostat B control unit. 100 mL of an overnight grown shake flask culture was used to inoculate the fermentor. For maintaining pH, 5 M NaOH was used. There was no correction for a too alkaline pH and fermentation started at pH 5.8 and was allowed to drop spontaneously until 3.5. Later unalterable incensement was seen as the end of the fermentation process. Feeding of rapeseed oil (Sigma) was started 48 h after inoculation, and was adjusted to the consumption rate. Additional glucose (50 g/L) was added 150 h after inoculation. Sophorolipids were extracted by the following procedure: 3 volumes of ethanol were added to the fermentation medium and yeast cells were removed by centrifugation. The water−ethanol mixture of the supernatants was removed under reduced pressure in a rotavapor. Two volumes of ethanol were added to dissolve the sophorolipids and the residual hydrophobic carbon source. The mixture was passed over a Whatman filter to remove the water-soluble components, and ethanol was evaporated under reduced pressure in a rotavapor. Solid substances were dissolved in water (pH 6.5), and residual oil and fatty acid were extracted by an equal volume of hexane. The sophorolipid mixture (about 80% C18:1) is comparable to what it was reported by other authors.[59] Finally, hydrolysis of the mixture to obtain the acidic COOH form of SL is performed with 5 M NaOH solution and extracted with pentanol according to the procedure described in ref 60. The product is then further purified on a chromatographic column using silica gel 60 as stationary phase and a 80:20 dichloromethane/methanol mixture. Thin-layer chromatography was performed on silica gel 60 plates (Whatman) using the same solvent mixture. Staining is done with phosphomolybdic acid (5 g in 50 mL ethanol solution), and revelation is performed by warming the substrate. Analysis is done with ^{1}H and ^{13}C NMR ($CDCl_3/CH_3OD$ = 1:1). An average downfield 5 ppm shift from 172 ppm to 177 ppm is used as reference to verify the ester hydrolysis of the COOH group. The final compound is mainly (>90%) constituted by acidic sophorolipids, as also verified by ^{1}H NMR (results not shown).

Sample Preparation. Different amounts of SL are added to D_2O (Aldrich) solutions at concentration c = 5, 50, 300, 400, and 500 mg/mL corresponding to volume fraction, Φ = 0.52%, 5.20%, 31.25%, 41.6%, and 52.08%. pH was increased using μmolar amounts of 0.5 and 1 M NaOH solutions, which were prepared in D_2O, in order to limit the incoherent scattering in SANS experiments. pH was measured with a classical pH-meter on the corresponding H_2O-based solutions. All samples, analyzed within 24 h from their preparation, are prepared well above the SL cmc, which is reported to be between 0.02 and 0.25 mg/mL.[61] In particular, Imura et al.[62] have reported a cmc value for the acidic form of SL of about 0.11 mg/mL. As for the fully ionized form (α = 1), we performed the measurement ourselves as cmc was never reported before under these conditions, to the best of our knowledge. Surface tension experiments (Figure S4 in the Supporting Information and related discussion) in H_2O as a function of the concentration of the fully ionized sophorolipid form provide a cmc value of about 0.15 ± 0.05 mg/mL, which is slightly higher but still comparable within error with the corresponding protonated form.

Experimental Techniques. Transmission electron microscopy under cryogenic conditions (Cryo-TEM) were run on two different microscopes. Lower resolution images in Figure 9 were taken on a FEI Tecnai 120 Twin microscope operating at 120 kV (magnification 30000 fold) and equipped with a high resolution Gatan Orius CCD 4k × 4k numeric camera. Higher resolution images in Figure 7 were obtained on a JEOL 2010F at the PFMU, Institut Pasteur (Paris, France). The microscope operates at 200 kV and magnification was 80.000 fold. A Gatan ultrascan 4000 camera was used to acquire the image. On both microscopes, DigitalMicrograph software was used for image acquisition. Cryofixation was either done on a EMGP, Leica (Austria) instrument or on a homemade cryo-fixation device. Liquid samples at desired concentrations were deposited on holey (10 μm) carbon coated TEM copper grids (Quantifoil R2/2, Quantifoil, Germany). Excess sample was eliminated, and the grid was immediately blotted into liquid ethane. All grids were kept at liquid nitrogen during storage and throughout all experimentation. Sample was observed with a Gatan Cryoholder (Gatan 626DH, Gatan).

Surface tension (γ) experiments were performed to evaluate the cmc using a Tracker tensiometer, from Teclis (France), in the needle pendant drop configuration. Values are collected as a function of time and averaged after equilibrium is reached.

^{1}H solution NMR spectra were acquired on a Bruker AV300 Ultrashielded Avance spectrometer equipped with a 5 mm (1H/BBF) BBO probe with *Z*-axis gradient using a standard 30° flip angle; intermolecular contacts were studied from a series of ^{1}H−^{1}H nuclear Overhauser effect spectroscopy (NOESY) NMR experiments with mixing times from 50 to 900 ms, performed with a standard three-pulse sequence.[45]

Small angle neutron scattering (SANS) was performed at the Léon Brillouin Laboratory (Orphée Reactor, Gif-sur-Yvette, France) on the PAXE beamline. The spectrometer configuration was adjusted to cover two different q-ranges. The small angle region $8.38.10^{-3}$ Å^{-1} < q < 7.32×10^{-2} Å^{-1} is obtained with a neutron wavelength, λ, of 6 Å and a sample-to-detector distance, D, of 5 m. An acquisition time of 4800 s was used; the medium angle region covers a q range 3.50×10^{-2} Å^{-1} < q < 2.80×10^{-1} Å^{-1} at λ = 6 Å with D = 1.20 m. An acquisition time of 1800 s was used in that case. Wavevectors lower than 8.38×10^{-3} Å^{-1} were obtained using D = 5 m and λ = 12 Å. q is defined as $4\pi/\lambda \sin \theta/2$, where θ is the scattering angle between the incident and the scattered neutron beams. All samples are introduced in a 2 mm quartz cell and studied at T = 22 °C. The blank sample is composed of 99.9% D_2O, whose signal is subtracted from the experimental data. Data treatment is done with the PAsiNET.MAT software package provided at the beamline and available free of charge.[63] Absolute values of the scattering intensity are obtained from the direct determination of the number of neutrons in the incident beam and the detector cell solid angle. The 2D raw data were corrected for the ambient background and empty cell scattering and normalized to yield an absolute scale (cross section per unit volume) by the neutron flux on the samples. The data were then circularly averaged to yield the 1-D intensity distribution, $I(q)$. The incoherent scattering was approximated from the high q intensity plateau and subtracted from the corresponding reduced data. Finally, data collected at the different configurations were used together without the need of introducing a correction factor, given the same acquisition wavelength under both configurations. *Scatter* software[64] was used to fit the form factor of selected SANS data sets using classical equations for sphere, cylinder, disk and vesicle models.[65] Ellipsoidal shape was derived from the cylindrical form factor. All fits were executed considering an homogeneous core system. The relationship between the scattering wavevector, q, and distance is $d = (2\pi/q)$. Relative considerations on the surface-to-volume ratio are done on the basis of the classical Porod law at high q:[65] $I(q)_{q=0} = \phi(2\pi/q^4)\Delta\rho S/V$, where $I(q)$ is the SANS measured intensity in absolute

scale, $\Delta\rho$ is the difference in the scattering length density between the solvent and the irradiated object, S is the total exposed surface, V is the total irradiated volume of all objects, and ϕ is the volume fraction.

Conflict of Interest: The authors declare no competing financial interest.

Acknowledgment. The research leading to these results has received funding from the European Community's Seventh Framework Programme (FP7/2007-2013) under Grant Agreement No. Biosurfing/289219. We thank G. Carrot (PAXE line, Laboratoire Léon Brillouin, Gif-sur-Yvette, France) for assistance on the PAXE beamline. M. Rawiso (Institut Charles Sadron, Strasbourg, France), M. Impéror-Clerc (Laboratoire de Physique du Solide, Université de Paris XII, Orsay), and F. Michaux (École Nationale Supérieure d'Agronomie et des Industries Alimentaires de Nancy, Nancy, France) are kindly acknowledged for helpful discussions on SANS. M. In (Laboratoire Charles Coulomb, Université de Montpellier II, France) is thoroughly acknowledged for his help in interpreting SANS data. M.-N. Rager (Ecole Nationale Supérieure de Chimie Paris, Paris, France) and F. Ribot (Laboratoire de Chimie de la Matière Condensée de Paris, Université Pierre et Marie Curie, Paris, France) are kindly acknowledged for helpful discussions on NMR experiments. Gervaise Mosser (Laboratoire de Chimie de la Matiére Condensée de Paris, Université Pierre et Marie Curie, Paris, France), for helping on cryo-TEM experiments. A. Salonen (Laboratoire de Physique des Solides, Université d'Orsay, France) is kindly acknowledged for providing access and support to surface tension experiments.

Supporting Information Available: Figure S1: results of the fit for SANS data of the SL/D_2O solutions. Table S1: numerical results from fits of SANS. Figure S2: results of the fit for SANS data for the 5 mg/mL and $\alpha = 1$ system. Figure S3: direct representation of the experimental structure factor and related discussion. Figure S4: surface tension experiments to determine the cmc value of the fully ionized ($\alpha = 1$) sophorolipid form. This material is available free of charge *via* the Internet at http://pubs.acs.org

REFERENCES AND NOTES

1. Xu, C.; Fu, X.; Fryd, M.; Xu, S.; Wayland, B. B.; Winey, K. I.; Composto, R. J. Reversible Stimuli-Responsive Nanostructures Assembled from Amphiphilic Block Copolymers. *Nano Lett.* **2006**, *6*, 2282–2287.
2. Jacquin, M.; Muller, P.; Cotter, H.; Théodoly, O. Self-assembly of charged amphiphilic diblock copolymers with insoluble blocks of decreasing hydrophobicity. *Langmuir* **2010**, *26*, 18681–18693.
3. Kawasaki, H.; Souda, M.; Tanaka, S.; Nemoto, N.; Karlsson, G.; Almgren, M.; Maeda, H. Reversible vesicle formation by changing pH. *J. Phys. Chem. B* **2002**, *106*, 1524–1527.
4. Lin, Y.; Han, X.; Huang, J.; Fu, H.; Yu, C. A Facile Route to Design pH-responsive Viscoelastic Wormlike Micelles: Smart Use of Hydrotropes. *J. Colloid Interface Sci.* **2009**, *330*, 449–455.
5. Chu, Z.; Feng, Y. pH-switchable Wormlike Micelles. *Chem. Commun.* **2010**, *46*, 9028–9030.
6. Negrini, R.; Mezzenga, R. pH-Responsive Lyotropic Liquid Crystals for Controlled Drug Delivery. *Langmuir* **2011**, *27*, 5296–5303.
7. Ray, S.; Das, A. K.; Banerjee, A. pH-Responsive, Bolaamphiphile-Based Smart Metallo-Hydrogels as Potential Dye-Adsorbing Agents, Water Purifier, and Vitamin B 12 Carrier. *Chem. Mater.* **2007**, *19*, 1633–1639.
8. Meister, A.; Bastrop, M.; Koschoreck, S.; Garamus, V. M.; Sinemus, T.; Hempel, G.; Drescher, S.; Dobner, B.; Richtering, W.; Huber, K.; et al. Structure-Properties Relationships in Stimuli-Responsive Bolaform Hydrogels. *Langmuir* **2007**, *23*, 7715–7723.
9. Meister, A.; Blume, A. Self-Assembly of Bipolar Amphiphiles. *Curr. Opin. Colloid Interf. Sci.* **2007**, *12*, 138–147.
10. Kjellin, M.; Johansson, I. *Surfactants from Renewable Resources*; John Wiley & Sons, Ltd.: West Sussex, 2010.
11. von Rybinski, W.; Hill, K. Alkyl Polyglycosides—Properties and Applications of a new Class of Surfactants. *Angew. Chem., Int. Ed.* **1998**, *37*, 1328–1345.
12. Stubenrauch, C. Sugar Surfactants – Aggregation, Interfacial, and Adsorption Phenomena. *Curr. Opin. Coll. Interf. Sci.* **2001**, *6*, 160–170.
13. Hoffmann, B.; Platz, G. Phase and Aggregation Behaviour of Alkylglycosides. *Curr. Opin. Coll. Interf. Sci.* **2001**, *6*, 171–177.
14. Baccile, N.; Nassif, N.; Malfatti, L.; Van Bogaert, I. N. A.; Soetaert, W.; Pehau-Arnaudet, G.; Babonneau, F. Sophorolipids: a Yeast-Derived Glycolipid as Greener Structure Directing Agents for Self-Assembled Nanomaterials. *Green Chem.* **2010**, *12*, 1564–1567.
15. Rau, U.; Hammen, S.; Heckmann, R.; Wray, V.; Lang, S. Sophorolipids: a Source for Novel Compounds. *Ind. Crops Prod.* **2001**, *13*, 85–92.
16. Tulloch, A. P.; Hill, A.; Spencer, J. F. T. Structure and Reactions of Lactonic and Acidic Sophorosides of 17-Hydroxyoctadecanoic Acid. *Can. J. Chem.* **1968**, *46*, 3337–3351.
17. Asmer, H.-J.; Lang, S.; Wagner, F.; Wray, V. Microbial Production, Structure Elucidation and Bioconversion of Sophorose Lipids. *J. Am. Oil Chem. Soc.* **1988**, *65*, 1460–1466.
18. Zhou, S.; Xu, C.; Wang, J.; Gao, W.; Akhverdiyeva, R.; Shah, V.; Gross, R. Supramolecular Assemblies of a Naturally Derived Sophorolipid. *Langmuir* **2004**, *20*, 7926–7932.
19. Develter, D. W. G.; Fleurackers, S. J. J. *Surfactants from Renewable Resources*; John Wiley & Sons, Ltd.: West Sussex, 2010; pp 213–238.
20. Maingault, M. Use of Sophorolipids and Cosmetic and Dermatological Compositions, WO/1995/034282A.
21. Van Bogaert, I. N. A.; Saerens, K.; De Muynck, C.; Develter, D.; Soetaert, W.; Vandamme, E. J. Microbial Production and Application of Sophorolipids. *Appl. Microbiol. Biotechnol.* **2007**, *76*, 23–34.
22. Shete, A. M.; Wadhawa, G.; Banat, I. M.; Chopade, B. A. Mapping of Patents on Bioemulsifier and Biosurfactant: a Review. *J. Sci. Ind. Res.* **2006**, *65*, 91–11.
23. Fu, S. L.; Wallner, S. R.; Bowne, W. B.; Hagler, M. D.; Zenilman, M. E.; Gross, R.; Bluth, M. H. Sophorolipids and Their Derivatives are Lethal Against Human Pancreatic Cancer Cells. *J. Surg. Res.* **2008**, *148*, 77–82.
24. Ishigami, Y.; Gama, Y.; Nagahora, H.; Yamaguchi, M.; Nakahara, H.; Kamata, T. The pH Sensitive Conversion of Molecular Aggregates of Rhamnolipid Biosurfactant. *Chem. Lett.* **1987**, 763–766.
25. Kitamoto, D.; Morita, T.; Fukuoka, T.; Konishi, M.; Imura, T. Self-Assembling Properties of Glycolipid Biosurfactants and Their Potential Applications. *Curr. Opin. Coll. Interf. Sci.* **2009**, *14*, 315–328.
26. Masuda, M.; Shimizu, T. Lipid Nanotubes and Microtubes: Experimental Evidence for Unsymmetrical Monolayer Membrane Formation from Unsymmetrical Bolaamphiphiles. *Langmuir* **2004**, *20*, 5969–5977.
27. By degree of ionization we refer to the ratio between COO^- and COOH groups, as defined in eq1 and discussed in the related paragraph.
28. Zimmels, Y.; Lin, I. J. Stepwise Association Properties of Some Surfactant Aqueous Solutions. *Colloid Polym. Sci.* **1974**, *252*, 594–612.
29. Maeda, H.; Eguchi, Y.; Suzuki, M. Hydrogen Ion Titration of Oleic Acid in Aqueous Media. *J. Phys. Chem.* **1992**, *96*, 10487–10491.
30. Bendejacq, D.; Joanicot, M.; Ponsinet, V. Pearling Instabilities in Water-Dispersed Copolymer Cylinders With Charged Brushes. *Eur. Phys. J. E* **2005**, *17*, 83–92.
31. Reiss-Husson, F.; Luzzati, V. The Structure of the Micellar Solutions of Some Amphiphilic Compounds in Pure Water as Determined by Absolute Small-Angle X-Ray Scattering Techniques. *J. Phys. Chem.* **1964**, *68*, 3504–3511.
32. Ekwall, P.; Mandel, L.; Solyom, P. The Aqueous Cetyltrimethylammonium Bromide Solutions. *J. Colloid Interface Sci.* **1971**, *35*, 519–528.

33. Quirion, F.; Magid, L. J. Growth and Counterion Binding of Cetyltrimethylammonium Bromide Aggregates at 25 Degree: a Neutron and Light Scattering Study. *J. Phys. Chem.* **1986**, *90*, 5435–5441.
34. Goyal, P. S.; Dasannacharya, B. A.; Kelkar, V. K.; Manohar, C.; Srinivasa Rao, K.; Valaulikar, B. S. Shapes and Sizes of Micelles in CTAB Solutions. *Physica B* **1991**, *174*, 196–199.
35. Kuperkar, K.; Abezgauz, L.; Danino, D.; Verma, G.; Hassan, P. A.; Aswal, V. K.; Varade, D.; Bahadur, P. Viscoelastic Micellar Water/CTAB/$NaNO_3$ Solutions: Rheology, SANS and Cryo-TEM Analysis. *J. Colloid Interface Sci.* **2008**, *323*, 403–409.
36. Glatter, O.; Fritz, G.; Lindner, H.; Brunner-Popela, J.; Mittelbach, R.; Strey, R.; Egelhaaf, S. U. Nonionic Micelles Near the Critical Point: Micellar Growth and Attractive Interaction. *Langmuir* **2000**, *16*, 8692–8701.
37. Shrestha, R. G.; Shrestha, L. K.; Sharma, S. C.; Aramaki, K. Phase Behavior and Microstructures of Nonionic Fluorocarbon Surfactant in Aqueous Systems. *J. Phys. Chem. B* **2008**, *112*, 10520–10527.
38. Hickl, P.; Ballauff, M.; Jada, A. Small-Angle X-ray Contrast-Variation Study of Micelles Formed by Poly(styrene)−Poly(ethylene oxide) Block Copolymers in Aqueous Solution. *Macromolecules* **1996**, *29*, 4006–4014.
39. Zhang, R.; Marone, P. A.; Thiyagarajan, P.; Tiede, D. M. Structure and Molecular Fluctuations of n-Alkyl-β-d-glucopyranoside Micelles Determined by X-ray and Neutron Scattering. *Langmuir* **1999**, *15*, 7510–7519.
40. Milkereit, G.; Garamus, V. M.; Veermans, K.; Willumeit, R.; Vill, V. Structures of Micelles formed by Synthetic Alkyl glycosides with Unsaturated alkyl Chains. *J. Colloid Interface Sci.* **2005**, *284*, 704–713.
41. Sodermann, O.; Johansson, I. Polyhydroxyl-Based Surfactants and Their Physico-Chemical Properties and Applications. *Curr. Opin. Coll. Interf. Sci* **2000**, *4*, 391–401.
42. Kwon, S. Y. Length Control in Rigid Cylindrical Nanoassembly by Tuning Molecular Interactions in Aqueous Solutions. *Langmuir* **2008**, *24*, 10674–10679.
43. Shimizu, T.; Masuda, M.; Minamikawa, H. Supramolecular Nanotube Architectures Based on Amphiphilic Molecules. *Chem. Rev.* **2005**, *105*, 1401–1443.
44. Imae, T.; Funayama, K.; Krafft, M. P.; Giulieri, F.; Tada, T.; Matsumoto, T. Small-Angle Scattering and Electron Microscopy Investigation of Nanotubules Made from a Perfluoroalkylated Glucophospholipid. *J. Colloid Interface Sci.* **1999**, *212*, 330–337.
45. Ernst, R. R.; Bodenhausen, G.; Wokaun, A. *Principles of Nuclear Magnetic Resonance in One and Two Dimensions*; Oxford University Press: New York, 1987.
46. Macura, S.; Ernst, R. R. Elucidation of Cross Relaxation in Liquids by Two-Dimensional N.M.R. Spectroscopy. *Mol. Phys.* **1980**, *41*, 95.
47. Zhao, J.; Fung, M. Conformational Change of Hydrocarbon Chains Upon the Formation of Micelles. *J. Phys. Chem.* **1993**, *97*, 5185–5187.
48. Yuan, H.-Z.; Cheng, G.-Z.; Zhao, S.; Miao, X.-J.; Yu, J.-Y.; Shen, L.-F.; Du, Y.-R. Conformational Dependence of Triton X-100 on Environment Studied by 2D NOESY and 1H NMR Relaxation. *Langmuir* **2000**, *16*, 3030–3035.
49. Aydogan, N.; Abbott, N. L. Interfacial Properties of Unsymmetrical Bolaform Amphiphiles with One Ionic and One Nonionic Head Group. *J. Colloid Interface Sci.* **2001**, *242*, 411–418.
50. Kan, P. L.; Papahadjopoulos-Sternberg, B.; Wong, D.; Waigh, R. D.; Watson, D. G.; Gray, A. I.; McCarthy, D.; McAllister, M.; Scha1tzlein, A. G.; Uchegbu, I. F. Highly Hydrophilic Fused Aggregates (Microsponges) from a C12 Spermine Bolaamphiphile. *J. Phys. Chem. B* **2004**, *108*, 8129–8135.
51. The theoretical OA chain length is calculated with $l = 1.5 + 1.265n$, where l is the chain length in Å and n is the number of CH_2 groups (see ref 52).
52. Tanford, C. *The Hydrophobic Effect: Formation of Micelle and biological Membranes*; John Wiley & Sons, Ltd.: New York, 1980.
53. Abel, S.; Dupradeau, F.-Y.; Raman, E. P.; MacKerell, A. D., Jr.; Marchi, M. Molecular Simulations of Dodecyl-β-maltoside Micelles in Water: Influence of the Headgroup Conformation and Force Field Parameters. *J. Phys. Chem. B* **2011**, *115*, 487–499.
54. Kaibara, K.; Iwata, E.; Eguchi, Y.; Suzuki, M.; Maeda, H. Dispersion Behavior of Oleic Acid in Aqueous Media: From Micelles to Emulsions. *Colloid Polym. Sci.* **1997**, *275*, 777–783.
55. OM=[(*cis*-9-octadecenyl)-4-*O*-(α-glucopyranosyl)-β-D-glucopyranoside)] has a chemical structure very close to SL.
56. de Koster, C. G.; Heerma, W.; Pepermans, H. A. M.; Groenewegen, A.; Peters, H.; Haverkamp, J. Tandem Mass Spectrometry and Nuclear Magnetic Resonance Spectroscopy Studies of *Candida bombicola* Sophorolipids and Product Formed on Hydrolysis by Cutinase. *Anal. Biochem.* **1995**, *230*, 135–148.
57. Das, S.; Bhirud, R. G.; Nayyar, N.; Narayan, K. S.; Kumar, V. V. Chemical Shift Changes on Micellization of Linear Alkyl Benzenesulfonate and Oleate. *J. Phys. Chem.* **1992**, *96*, 7454–7457.
58. Lang, S.; Brakemeier, A.; Heckmann, R.; Spockner, S.; Rau, U. Production of Native and Modified Sophorose Lipids. *Chim Oggi-Chem. Today* **2000**, *18*, 76–79.
59. Davila, A.-M.; Marchal, R.; Vandecasteele, J.-P. Sophorose Lipid Production from Lipidic Precursors − Predictive Evaluation of Industrial Substrates. *J. Ind. Microbiol.* **1994**, *13*, 249–257.
60. Rau, U.; Heckmann, R.; Wray, V.; Lang, S. Enzymatic Conversion of a Sophorolipid into a Glucose Lipid. *Biotechnol. Lett.* **1999**, *21*, 973–977.
61. Develter, D. W. G.; Lauryssen, L. M. L. Properties and Industrial Applications of Sophorolipids. *Eur. J. Lipid Sci. Technol.* **2010**, *112*, 628–638.
62. Imura, T.; Masuda, Y.; Minamikawa, H.; Fukuoka, T.; Konishi, M.; Morita, T.; Sakai, H.; Abe, M.; Kitamoto, D. Enzymatic Conversion of Diacetylated Sophoroselipid into Acetylated Glucoselipid: Surface-Active Properties of Novel Bolaform Biosurfactants. *J. Oleo. Sci.* **2010**, *59*, 495–501.
63. http://didier.lairez.fr/dokuwiki/doku.php?id=pasinet.
64. Förster, S.; Burger, C. Scattering Functions of Polymeric Core−Shell Structures and Excluded Volume Chains. *Macromolecules* **1998**, *31*, 879–891.
65. Glatter, O.; Kratky, O. *Small Angle X-ray Scattering*; Academic Press: London, 1982.